2023-07

Monitoring of drying kinetics evolution and hygrothermal properties of new earth-based materials using climatic chamber simulation

Azil, A

10.1016/j.cscm.2022.e01798
Case Studies in Construction Materials
Elsevier BV

Case Studies in Construction Materials 18 (2023) e01798

Contents lists available at ScienceDirect

Case Studies in Construction Materials

journal homepage: www.elsevier.com/locate/cscm

Case study

Monitoring of drying kinetics evolution and hygrothermal properties of new earth-based materials using climatic chamber simulation

Athmane Azil [a,*], Karim Touati [a], Nassim Sebaibi [a], Malo Le Guern [a], François Streiff [b], Steve Goodhew [c], Moussa Gomina [d], Mohamed Boutouil [a]

[a] ComUE Normandie Université, Builders Ecole d'Ingénieurs, Builders Lab 1, Rue Pierre et Marie Curie, 14610 Epron, France
[b] Parc Naturel Régional des Marais du Cotentin et du Bessin (PnrMCB), France
[c] University of Plymouth, United Kingdom
[d] Laboratoire CRISMAT, UMR 6508 CNRS, ENSICAEN, 6 bd Maréchal Juin, CEDEX 4, Caen 14050, France

ARTICLE INFO

Keywords:
Drying kinetics
Hygrothermal properties
Cob
Light-earth
Water content
Thermal conductivity

ABSTRACT

This study focuses on the drying kinetics of cob and light-earth layers comprising a hybrid walling system. Volumetric water content sensors are immersed and placed at different positions on the walls of a building to measure the drying kinetics. In addition, an experimental analysis of the effect of temperature, relative humidity (RH), and wind velocity variations on thermal conductivity in a climatic chamber under winter and summer conditions was conducted. The analysis of samples in laboratory aims to investigate the hygrothermal properties of cob and light-earth materials, and their dependency on the aforementioned parameters. The *in situ* drying kinetics of both materials involves water content reduction and stabilization; however, in the laboratory, although the water content of materials decreases, the drying is incomplete. Which may be due to the limited wind speed. The hydrothermal properties show that open porosity affects water vapor permeability and modifies the RH of cob and light-earth. At 23 °C, when the relative humidity (RH) range was 10–30%, the absorbed water vapor of cob and light earth was 0–2%. However, when the RH is 40–90%, the absorbed water vapor of light earth (2–9%) exceeds that of cob (0.5–2%). Moreover, the response to relative humidity (RH) with regard to the mixing law of components and samples differs. The resistance factor to water vapor diffusion values for cob and light-earth are 12.9 and 8.2, respectively. In this study, the thermal conductivity measurements under summer and winter conditions provide the relationship between the thermal conductivity, density, and water content of cob and light-earth materials.

Abbreviations: d_a, air layer thickness (m); E, sample thickness (m); g, vapor flux density ($kg \bullet m^{-2} \bullet s^{-1}$); t, time (s); A, sample exposed area (m^2); G, water vapor flux ($kg \bullet s^{-1}$); W_L, liquidity limit (%); I_p, plasticity index (%); MBV, methylene blue value (g/100 g); M_{air}, mass of saturated sample in air (kg); M_{oil}, mass of saturated sample in non-wetting oil (kg); M_{dry}, mass of dry sample (kg); M_t, total mass (kg); W_m, water content mass by mass (%); W_{owc}, optimum water content (%); $W_{Absorption}$, absorption coefficient (%); RH, relative humidity (%); W, water vapor permeance ($kg.m^{-2} \bullet s^{-1} \bullet Pa^{-1}$); W_c, corrected water vapor permeance ($kg.m^{-2} \bullet s^{-1} \bullet Pa^{-1}$); Z_a, air layer water vapor resistance (m^2.s. Pa/kg); Z, water vapor resistance ($m^2 \bullet s \bullet Pa/kg$); ΔP_v, difference in water vapor partial pressure (Pa); δ, sample water vapor permeability ($kg \bullet m^{-1} \bullet s^{-1} \bullet Pa^{-1}$); δ_a, water vapor permeability of air ($kg \bullet m^{-1} \bullet s^{-1} \bullet Pa^{-1}$); μ, water vapor resistance factor (-); ∅, diameter of cylindrical samples (mm); H, height of cylindrical samples (mm); $\rho_{Absolute}$, absolute density (kg/m^3); ρ, bulk density (kg/m^3); γ_{dmax}, maximum dry density (kg/m^3); Φ, open porosity (%); λ, thermal conductivity ($W \cdot m^{-1} \cdot K^{-1}$); T, temperature (°C).

* Corresponding author.
E-mail address: azil.athmane@gmail.com (A. Azil).

https://doi.org/10.1016/j.cscm.2022.e01798
Received 11 July 2022; Received in revised form 30 November 2022; Accepted 20 December 2022
Available online 21 December 2022

1. Introduction

The term "building material" refers to any material used in construction work. Different types of materials have been used in construction, and among the oldest in the world are earth-based materials containing bio-aggregates. Today, one-third of the world's population continues to reside in earth housings; half of these dwellings are found in developing countries [1]. These materials are relevant in the field of construction because of their low environmental impact and carbon footprint.

Earth-based materials are made from natural raw materials, mainly from local soils and agricultural products. Similarly, raw earth is local resource with an extremely low embodied energy [2]. It requires simple *in situ* production processes [3,4] and exhibits a wide variety of advantageous properties, rendering it ecologic in nature and non-polluting. It can also contribute to the temperature and moisture control in buildings [5]. Earth-based construction has many forms, including adobes, compressed earth bricks, rammed earth, and cobs. In this regard, cob building contain bio-aggregates is a traditional technique that has been implemented worldwide under various climates [6].

One of the major advantages of earth-based materials is their hygroscopic nature. This characteristic is particularly relevant when considering the potential harmful effects of humid environments on human health [7]. Humid environments can also damage buildings in terms of accelerated aging [8–10]. Furthermore, Moisture reduce the thermal performance of materials, but if you use hygroscopic materials your aim is to have them absorbing moisture to make the environment more comfortable [10,11]. At present, earthen construction remains the most widely used construction technique in the world.

The research on bio-based and earth-based materials is typically focused on mechanical performance [12–17,35], durability [18,19], and shrinkage [20–22]. However, these materials offer other benefits that are important to study, specifically those related to hygrothermal properties and thermal performance.

In recent years, researchers have been interested in hygrothermal properties. They have conducted experimental studies to compare the thermal conductivity values of earth-based materials [23–29]. The study of the water vapor permeability of earth-based materials has been extremely limited. Although research on hygrothermal properties has been implemented [24,30,31], few studies have been conducted on the hygrothermal properties of cob and light-earth. The water vapor resistance factor (μ) and thermal conductivity (λ) of different earth-based materials are listed in Table 1.

The thermal conductivity range of cob is 0.45–0.93 $W \bullet m^{-1} \bullet K^{-1}$ [1,34], and that of light-earth is 0.11–0.14 $W \bullet m^{-1} \bullet K^{-1}$ [16,34] depending on the porosity, density, nature of fibers, and water content. Nevertheless, knowledge of a single characteristic may not be sufficient to represent the hydrothermal behavior and thermal performance of a material. Temperature [36] and moisture content due to hygroscopic behavior [37] are known to impact the thermal properties of materials during the variation in the climatic boundary conditions. Numerous pores of materials are filled with water and air that can increase or decrease the thermal conductivity, resulting in the presence of three phases: solid matrix, air, and water. In addition, the competition among the effects of these phases determines the effective thermal properties of earth-based materials [11]. Hence, open porosity must be investigated to understand its impact on hygrothermal properties [38]. To accomplish this goal, an EU Interreg project called CobBauge was conducted. This project focuses on developing, testing, and establishing new low-carbon materials using local soil and vegetal fibers.

This study investigates the effect of temperature and relative humidity (RH) variations on drying kinetics and thermal conductivity cob and light-earth building materials, under winter and summer conditions using a climatic chamber simulation. Also, *in situ* studies of drying kinetics (in cob and light earth constituting the walls of a CobBauge prototype building) will be undertaken. This will help in understanding the drying process in such constructions. Moreover, the study compares the observations in this chamber with data obtained *in situ*. Also, an experimental procedure was implemented to investigate the hygrothermal properties of the cob and light-earth building materials used in the construction of the prototype structure [39,40]. (Fig. 1).

This paper is articulated in five sections.

1. Introduction of the study;
2. Materials and methods adopted in the experimental investigation;
3. Results and discussions;
4. Literature comparison;
5. Conclusion.

Table 1
Water vapor resistance factor (μ) and thermal conductivity (λ) reported in literature.

Authors	Material	Dry density ($kg.m^{-3}$)	μ (-)	λ ($W \cdot m^{-1} \cdot K^{-1}$)
Allinson et al.[30]	Rammed earth	1900	14.34	0.643
Cagnon et al.[24]	Earth bricks	1940–2070	7–9	0.40–0.69
Liuzzi et al.[23]	Hydrated lime–stabilized clay composites	1829–2046	8.10–11.10	0.74–1.2
Colinart et al.[28]	Light-earth	190–353	2.24–4.14	0.06–0.12
Labat et al.[5]	Light-earth	241–531	4.8	0.07–0.12
Volhard[32]	Light-earth	300–1200	2–5	0.1–0.47
Niang et al.[33]	Typha–clay composite	323–586	3.75–7.06	0.065–0.112

2. Materials and methods

In situ and in laboratory experimental program developed in this research paper are summarized in Fig. 2, with Cob and light earth materials.

2.1. Raw earth

Classical geotechnical characterization was performed on three soil samples collected from Normandy. Clay was evaluated according to the methylene blue value test (NF P94–068) [41] and Atterberg's limit (NF EN ISO 17892–12) [42].

The characteristics obtained using the foregoing tests enabled the classification of soils using the NF P11–300 standard [43] (See Table 2).

The specific density was evaluated using a helium pycnometer (Accupyc II 1340) according to ISO standard 17892–3 [44].

The particle size distribution was evaluated by mechanical wet-sieving for particles exceeding 80 μm according to the XP P94–041 standard [45] (Fig. 3) and by laser granulometry for particles less than 80 μm according to ISO standard 13320 [46].

The results of the standard Proctor compaction test [47] for the three soils are shown in Fig. 4. The figure indicates that the maximum dry density (γ_{dmax}) and optimum water content (W_{owc}) of soil 2 are 1827 kg/m^3 and 14%, respectively, and those of soil 3 are 1771 kg/m^3 and 15.83%, respectively. However, the dry density and optimum water content of soil 1, 2034 kg/m^3 and 9.7%, are higher and lower than those of the two soils previously mentioned, respectively.

2.2. Vegetal fibers

Two fibers were tested in this work: flax straw and reed fibers (maximum length: 6 cm). To measure their quantitative lengths, Image J software, (Fig. 5) was used. A digital image of fibers is composed of pixels. One of the first classical operations is therefore to convert the size of the pixels into physical length. Which also allows automatic detection and analysis of the real length of (50) fibers.

After drying and stabilization, the specific density of the fibers was determined using a helium pycnometer (Accupyc II 1340) [44], and the water absorption capacity was measured according to the RILEM protocol [49]. The fiber properties are listed in Table 3. Results presented in this table represent an average of three measurements.

After 24 h, the water absorption capacities of the flax straw and reed fibers were 350% and 198% compared to dry weight, respectively. The water absorption capacity of these fibers influences the mix properties in the long-term (hygrometric balance) and fresh states of cob and light earth materials.

2.3. Mixes and sample preparations

Experiments were performed on earth-based materials consisting of mixes of earth, water, and vegetal fibers. Before the preparation of cob and light-earth samples, the soils were screened through a 20-mm sieve according to the NF P94–093 standard [13]. Then, the soils and vegetal fibers were dried in an oven heated to 40 °C [50]. Cob material was obtained by mixing silty clay, sandy silt, and flax straw with an initial mass water content of 20%. The cob was rested for 24 h before the samples were prepared, to allow the moisture content to be evenly spread throughout the sample. Light-earth material was obtained by mixing elastic silt and reed fiber with an initial mass water content of 90%. The mix formulations are summarized in.

Table 4. To achieve the objectives of the study, three cylindrical (⌀110 mm × H220 mm) and four prismatic (300 × 300 × 70 mm) samples were prepared (Fig. 6) by normal proctor compaction (NF P94–093) [13] using 0.6 and 0.2 MJ/m^3 for cob and light-earth,

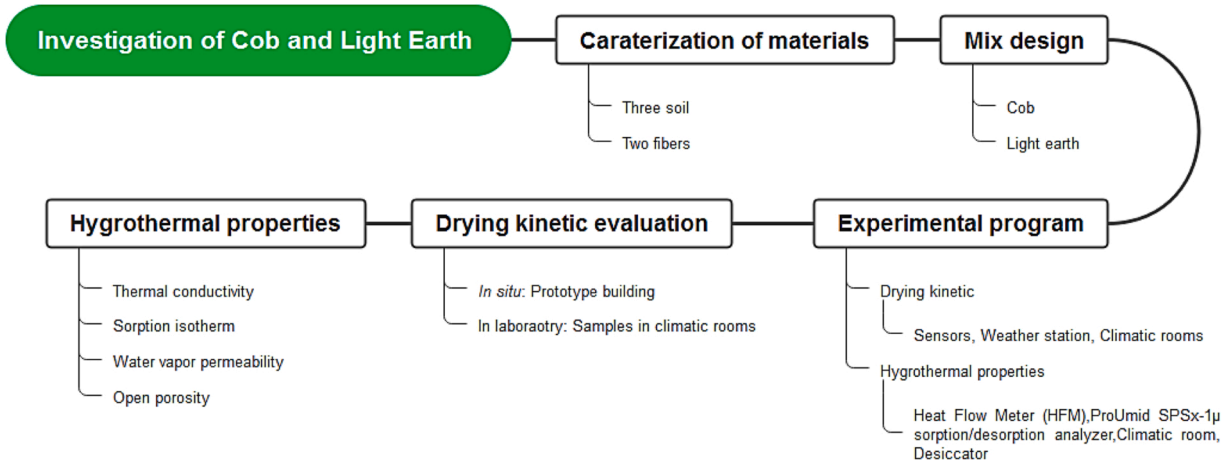

Fig. 1. Structure of research paper.

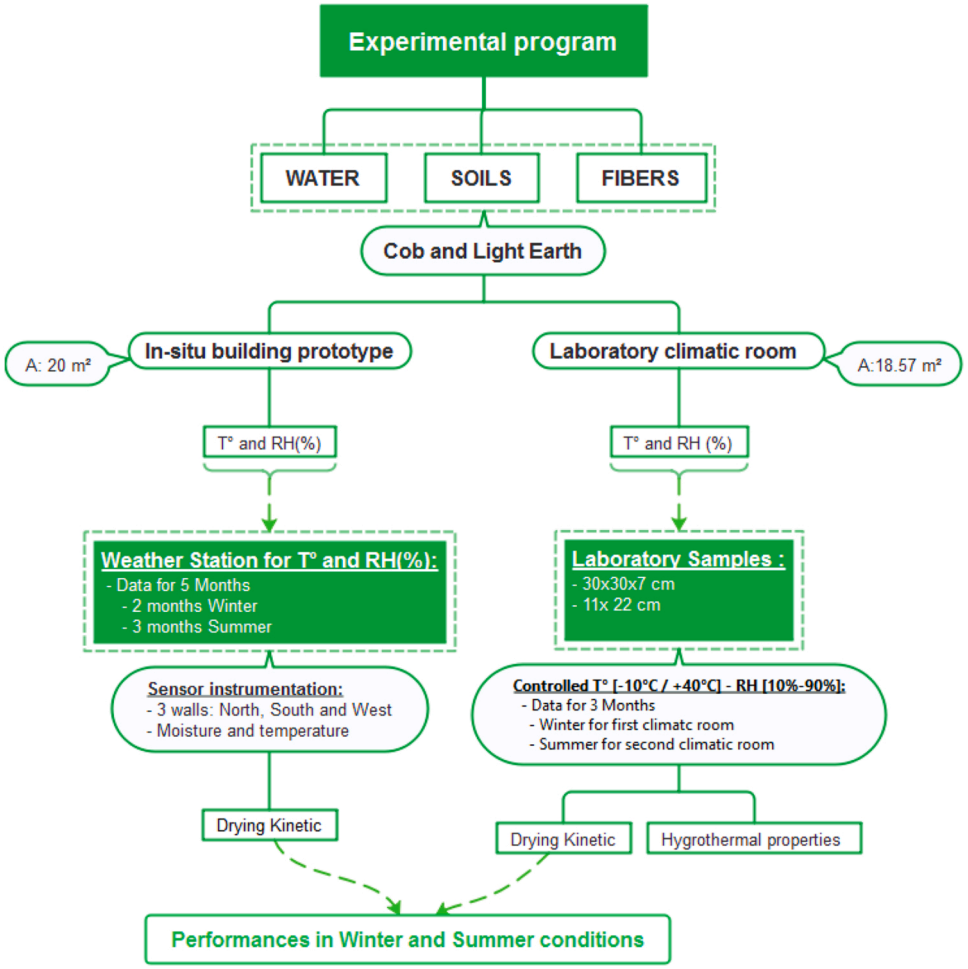

Fig. 2. Experimental program.

Table 2
Soils properties.

Soils	Soil 1	Soil 2	Soil 3
Liquidity limit (%)	22.8	28.5	57.4
Plasticity index (%)	2.3	4.2	14.9
Methylene blue value (g/100 g)	0.46	1.78	6.49
Particles < 80 μm (%)	20	90	80
$\rho_{specific}$ (kg/m^3)	2603 ± 1	2671 ± 2	2567 ± 1
Nature of soil (NF P11–300)	Low-plasticity silt	Fine clay sand	Highly plastic clay

respectively.

After compaction, the cylindrical samples were maintained at 20 ± 2 °C and 50 ± 5% RH for 1 d and then dried at 40 ± 2 °C [36] until equilibrium was attained (three consecutive weights were obtained at 24-h intervals with a standard deviation of 1%). Bulk density was determined according to the NF X31–501 standard [51]. The prismatic samples were placed in climatic chambers at different temperatures and relative humidities (Fig. 6).

2.4. In situ weather station and laboratory "climatic chamber" investigation

A weather station (WS-GP1) is installed near a 20-m^2 the prototype building CobBauge (cob and light earth dual-layer wall) prototype building in Normandy (France) (See Fig. 7). It determines the influence of outdoor environment during the construction and service life of the building. The WS-GP1 automatic weather station is equipped with sensors for measurements on the following parameters: wind velocity and direction, rainfall, solar radiation, relative humidity, and air temperature. The system comes complete

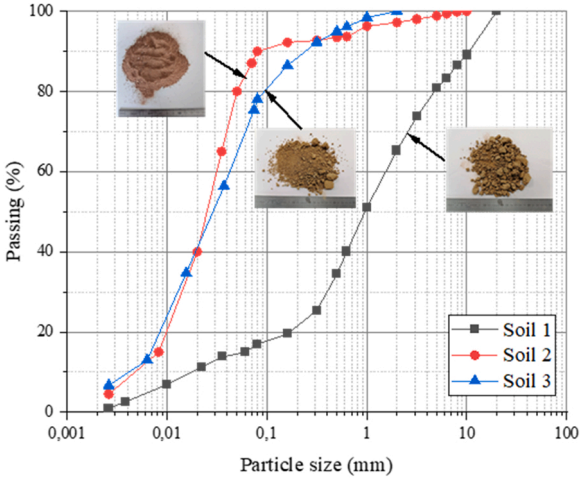

Fig. 3. Soil particle size distribution.

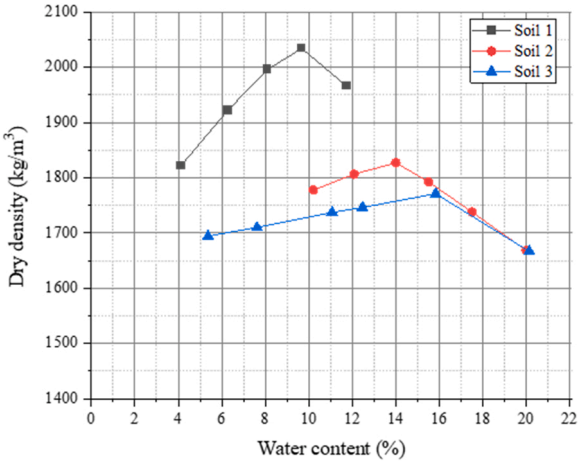

Fig. 4. Standard Proctor compaction curve for soils [48].

with the GP1 data logger and a 2-meter tripod mast. The sensors are reliable and suitable for use in extreme environments. The internal battery provides 6 months of operation (typical, for an alkaline battery), with 15 min sampling interval measurement.

The average temperature and RH in winter and summer were measured by the weather station (Table 5 and Fig. 8). The daily mean values of RH and temperature were calculated based on the hourly data obtained from weather station.

The goal is investigated the both materials in two climatic chambers based on the reproduction of three parameters: *mean temperature*, *mean relative humidity* of the weather station under winter and summer conditions and *wind speed*. The dimensions of these climatic chambers are: Hight: 3.75 m, Depth: 5.09 m and width: 3.65 m, which represents a volume of 69 m^3, they can provide temperatures from − 15 °C to + 40 °C (± 0.1 °C), relative humidity from 10% to 95% (± 5%) and wind speed of 0.3 $m \bullet s^{-1}$.

2.5. *Wall moisture monitoring*

Techniques based on the knowledge of dielectric permittivity are typically used to control the water content in soils. The dielectric permittivity property is highly dependent on the water content of a material.

To determine the water content, *in situ* methods based on the principle of reflectometry are preferred because of their robustness and ease of use. In this study, Campbell Scientific CS655 sensors based on the reflectometry principle were employed to measure the volumetric water content (VWC) locally. This type of sensor has already been proven to be effective in measuring the water content of soil-based materials [52,53]; its accuracy is ± 3% (± 1% with soil-specific calibration). To monitor the moisture contents of cob and light-earth layers comprising a wall, the sensors are placed at same height and depth in the materials (Fig. 9). The CS 655 sensors were placed horizontally to ensure better contact between the mixtures and rods as well as to facilitate implementation. The probes were positioned parallel to the wall surfaces at two different heights, 25 and 50 cm, from the base of the lift. The data collected by the CS 655

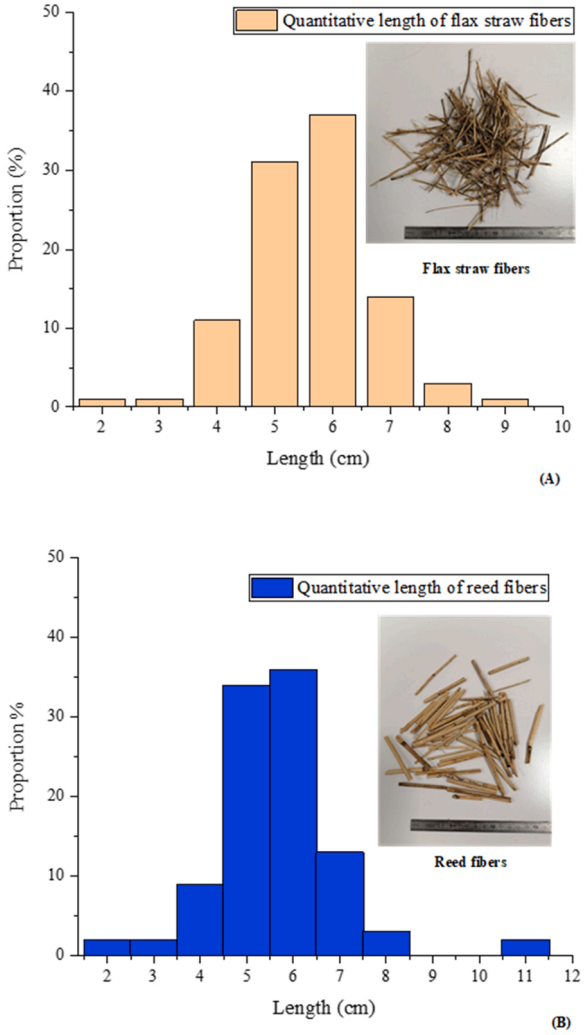

Fig. 5. Quantitative lengths of fibers: (A) flax straw and (B) reed fibers.

Table 3
Vegetal fiber properties.

Fibers	Flax straw	Reed
$W_{Absorption}$ at 24 h (%)	350 ± 11	198 ± 4
$\rho_{specific}$ (kg/m^3)	1266 ± 55	1305 ± 11

Table 4
Mix formulations.

Cob			Light-earth	
Soil 1 (wt%)	Soil 2 (wt%)	Flax straw fiber (wt%)	Soil 3 (wt%)	Reed fiber (wt%)
32.5%	65%	2.5%	65%	35%

sensors were stored in the CR1000X data logger every 15 min for more than one year (from 05/2020–11/2021).

2.6. *Experimental characterization of the samples*

To investigate the hygrothermal properties of materials, analyzing their interactions with water vapor is essential. Two types of

Fig. 6. Samples prepared for (A) water vapor permeability with porosity testing and (B) thermal conductivity measurement.

Fig. 7. Prototype building in Normandy (France).

Table 5
Winter and summer conditions in weather station and climatic chamber.

		Winter		Summer	
Weather station	Period	From 01/14/2020–02/29/2020		From 06/01/2021–08/25/2021	
	Parameters	Temperature (°C)	RH (%)	Temperature (°C)	RH (%)
	Mean	5	80	20	80
	Wind speed	1.62 m•s^{-1}		0.9 m•s^{-1}	
Climatic chamber	Period	3 months		3 months	
	Parameters	Temperature (°C)	RH (%)	Temperature (°C)	RH (%)
	Mean	5 ± 2	80 ± 5	20 ± 2	80 ± 5
	Wind speed	0.3 m•s^{-1}		0.3 m•s^{-1}	

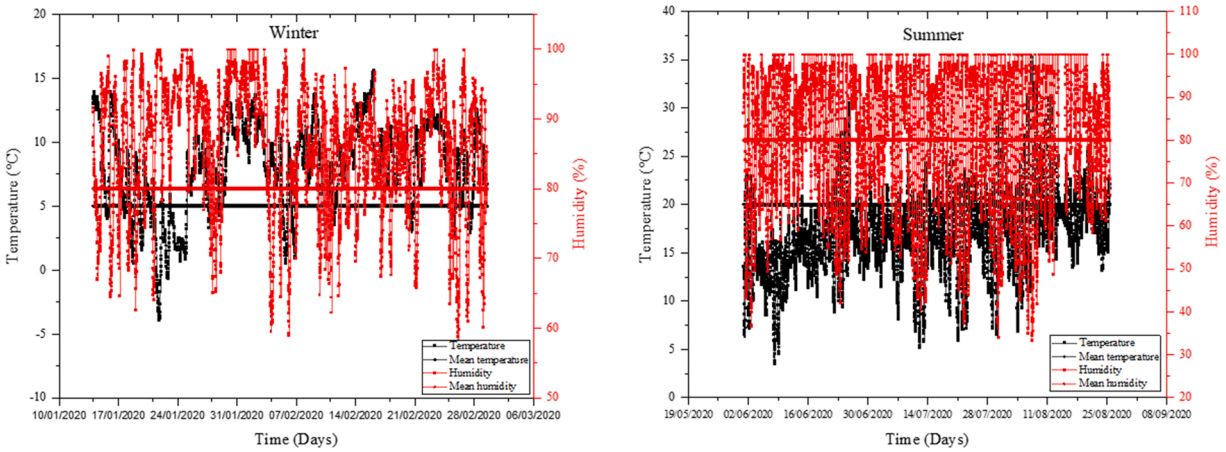

Fig. 8. Temperature and RH in winter and summer measured by weather station.

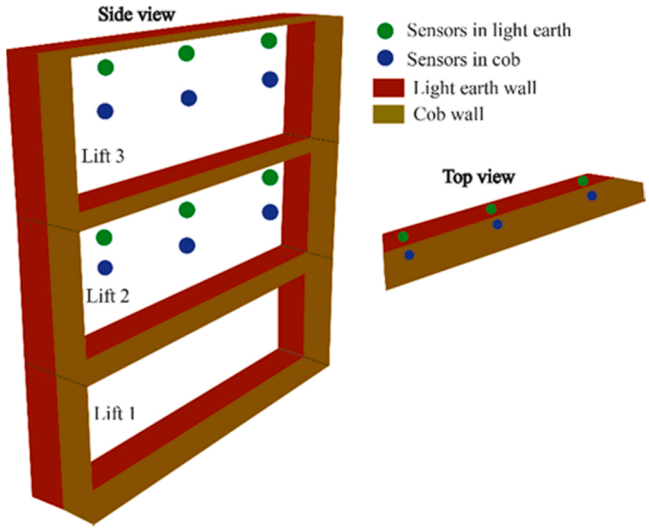

Fig. 9. Water content sensors in cob and light-earth layers.

tests were employed for the cob and light-earth materials: equilibrium water content using the dynamic vapor sorption (DVS) technique [54] and vapor permeability using the dry cup method [55]. Open porosity must also be measured to understand its impact on hygrothermal properties [38].

2.6.1. *Sorption isotherm*

The DVS technique was used to analyze the interaction between the material and water vapor. Three samples consisting of different soils, fibers, and mixes were analyzed. The sorption isotherms of these raw materials were studied according to the ISO 12571 standard [54]. Before the adsorption analysis was implemented, the samples were dried at 40 ± 2 °C [56] until reaching equilibrium (three consecutive weights at 24 h intervals within a standard deviation of 1%). Then, the ProUmid SPSx-1μ sorption/desorption system was utilized. The samples were exposed to 10–90% RH in five stages (25%, 40%, 50%, 70% and 90%) while maintaining the test temperature at 23 °C.

2.6.2. *Water vapor permeability*

To investigate the capacity of the material to allow vapor to pass through, water vapor permeability was measured. This parameter represents the ratio of the quantity of water vapor passing through a material ($kg \bullet m^{-1} \bullet s^{-1} \bullet Pa^{-1}$). The experimental procedure was applied to three cylindrical samples of each cob and light-earth material. The test was implemented according to the dry cup method, which was set up according to the NF ISO 12572 standard [55].

Before implementing the test, the samples 110 mm × H220 mm are cut into small samples 110 mm × H40 mm (Fig. 10) and kept in an environment where the temperature and RH were 20 ± 2 °C and 50 ± 5%, respectively. The test cup, sealed on the side with an

aluminum adhesive tape, was positioned at the top of the dish and held in place using a plastic holder (Fig. 10). Then, according to the relative humidity of the air inside and outside the cup, the mass of the samples was monitored until equilibrium was attained. The chosen the relative humidity of the air inside and outside the cup were 0% and 50% at 23 °C, respectively.

The previous provides information on material behavior when moisture transfer is dominated by vapor diffusion. Vapor flux through the material was determined by weighing the sample cup assembly. At a steady state, the water vapor flux (G) through the sample is given by the slope of the regression line of the sample cup assembly mass *vs* time. This was obtained after eliminating the initial nonlinear phase of the test. The flux or transmission of the water vapor rate (g) is calculated using Eq. (1).

$$g = \frac{G}{A}, \tag{1}$$

Where.

A: area of the sample (m^2);.

G: water vapor flux ($kg \bullet s^{-1}$).

Eq. (2) can be used to calculate the water vapor resistance (Z) from the water vapor permeability (W) depending on the difference in water vapor partial pressure (ΔP_v) between the two sides of the sample:

$$Z = \frac{1}{W} = \frac{A \times \Delta p_v}{G}. \tag{2}$$

Subsequently, the water vapor resistance of the air layer (Z_a) present in the measuring cup was obtained by determining the air layer thickness (d_a) and air water vapor permeability at an atmospheric pressure (δa) equal to 2×10^{-10} $kg \bullet m^{-1} \bullet s^{-1} \bullet Pa^{-1}$ using Eq. (3):

$$Z_a = \frac{d_a}{\delta_a}. \tag{3}$$

The corrected water vapor permeance, W_c, is obtained using Eq. (4):

$$W_c = \frac{1}{Z - Z_a}. \tag{4}$$

The water vapor permeability of the sample (δ) can then be determined using Eq. (5):

$$\delta = W_c \times E, \tag{5}$$

Where E is the sample thickness (m).

Finally, the water vapor resistance factor of the material (μ) is determined using Eq. (6):

$$\mu = \frac{\delta_a}{\delta}. \tag{6}$$

2.6.3. Open porosity

In this study, the open porosity was measured by immersing small samples in non-wetting oil (dearomatized oil) according to the NF ISO 5017 standard [57]. Then, the samples were oven-dried at 40 ± 5 °C, placed in a non-wetting oil-filled beaker, and saturated under vacuum in a desiccator for at least 24 h. This allowed the nonwetting oil to replace the air in the open pores without interacting with the sample volume. Subsequently, the samples were weighed in air and non-wetting oil (Fig. 11). The open porosity was determined according to Eq. (7):

Fig. 10. Experimental water vapor permeability test.

$$\Phi = \frac{M_{air} - M_{dry}}{M_{air} - M_{oil}} \times 100, \quad (7)$$

Where.

Φ is the open porosity (%);.

Mair is the mass of the saturated sample in air (kg);.

Moil is the mass of the saturated sample in the nonwetting oil (kg); and.

Mdry is the dry mass.

2.6.4. Thermal conductivity

The thermal conductivity, λ, of the cob and light-earth materials at different water contents under winter and summer conditions were measured in the laboratory (climatic chambers); the air speed was 0.3 m•s^{-1}. The experimental conditions in the climate-controlled chamber are listed in Table 5.

Thermal conductivity measurements were implemented on the prismatic samples (300 mm × 300 mm × 70 mm) of cob and light-earth materials (Fig. 6**B**).

A Netzsch HFM436 Lambda heat flux meter was used according to ISO 196 8301:1991 [51]. The results range from the initial water content value ($W_m = 20\%$ for cob and $W_m = 100\%$ for light earth) to the equilibrium water content value. The measurement of the heat flux through the materials involves generating a temperature gradient between two plates at a mean temperature of 20 °C (the cold and hot plates are at 10 and 30 °C, respectively). When the equilibrium state is reached and the heat flux is constant, the thermal conductivity of the material is calculated using Fourier's law [52].

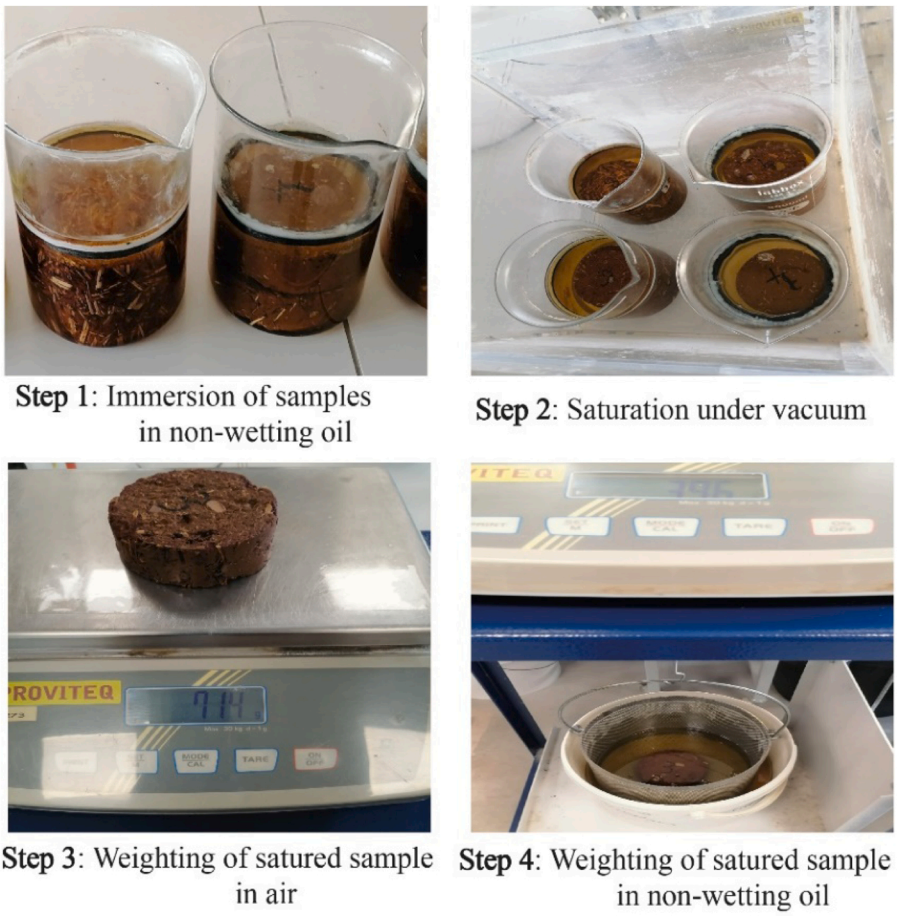

Fig. 11. Porosity measurement in cob and light-earth.

3. Results and discussions

3.1. In situ drying kinetics

The course of water content recorded by sensors in the cob and light-earth materials is shown in Fig. 12. In the cob layer, the VWC curves linear decreased in the initial days following the cob implementation *in situ*. After 25 d, when building an additional lift, the decrease in water content stopped (phase 1, Fig. 12). This can be explained by the fact that the amount of water from the new lift at the top of the existing lift was generally constant. After this brief period, the VWC curve decreased again; however, its slope was smaller than in the initial phase. The south and west walls are more exposed to wind. The corresponding VWC curve is linear and smaller than in the initial phase. On the north wall, a type of VWC stabilization is observed. This is temporary because radiation and temperature increase between March and August.

Fig. 12 presents two drying phases: an initial fast drying, where the slope is very steep, followed by a second phase with slower drying, going towards stabilization. Although this is a composite wall, this behavior is consistent with the typical phases observed in construction materials [58]: a first one that is faster, because of the liquid transport of water towards the drying surface. With water content getting lower, liquid transport diminishes and vapor transport gets more relevant, but the drying process gets slower. The VWC of the north wall follows a decreasing curve with a slope similar to those of the south and west walls (phase 2, Fig. 12).

In Fig. 13 (phase 1), the curves pertaining to the light-earth layer show large difference in the initial water content (even for the same lift). These changes can be attributed to the material preparation method and water addition by craftsmen during processing. Sometimes, light-earth material is directly used as the wall's formwork. Typically, however, it remains in big bags for a few hours before it is employed. This can lead to the loss of a quantity of water through evaporation and variations in water content during construction.

The VWC curve of the light-earth material decreases with a stiff slope after few stagnation days; this differs from the observed VWC curve of the cob material. In the latter, the VWC starts to decrease instantly after the material is implemented. In addition, in the case of light-earth material compared with the cob, the effect of adding a new lift on a dried lift is less evident. The fact that the light-earth is on the external side of the walls makes it more exposed and sensitive to variations in weather conditions. Between October and April, different peaks were observed in light-earth water content curves. The south and west walls are particularly affected, as shown in Fig. 13 (phase 2). Finally, it can be stated that light earth reaches the practical water content faster than cob. This can be due to different factors such as: initial water content, exposition to wind (light earth is more exposed), porosity, *etc.* Despite the differences, the materials still have a comparable drying behavior.

3.2. Laboratory drying kinetic

In climatic chambers under summer and winter conditions, the monitoring of water content variations by mass loss in the cob and light-earth materials is shown in Fig. 14 and Fig. 15, respectively.

In the first week, the drying kinetics of cob was the same (Phase 1, Fig. 14) due to the homogeneity; moreover, the material was undisturbed for 24 h. Then, with a difference of 2 – 4% in water content under winter and summer conditions, a decrease in drying kinetics was observed. After three months, the samples became dry with stable water contents of 2.1% and 0.8% in winter and summer, respectively (phase 2, Fig. 14).

In the first week, the drying kinetics of light earth changes with water content variation (91–125% in winter and 83–107% in summer (phase 1, Fig. 15). Then, with a difference of 4–20% in water content under the winter and summer conditions, a decrease in

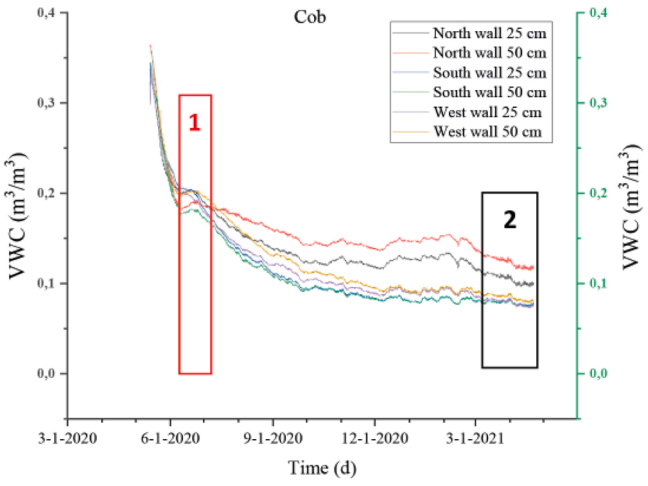

Fig. 12. In situ drying kinetics of cob material in north, south, and west walls.

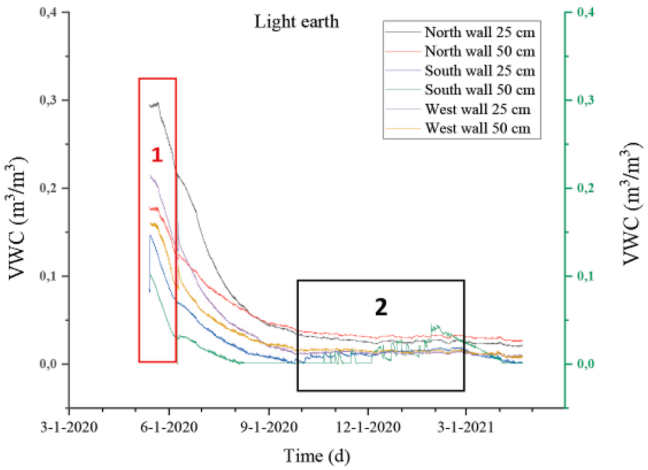

Fig. 13. In situ drying kinetics of light-earth material in north, south, and west walls.

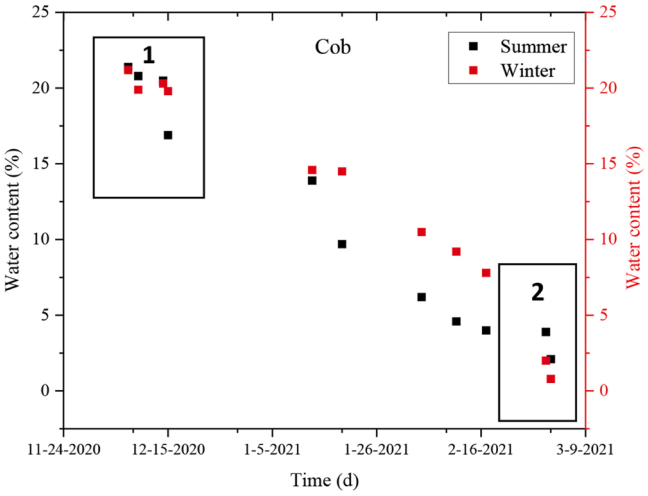

Fig. 14. Laboratory drying kinetics of cob material.

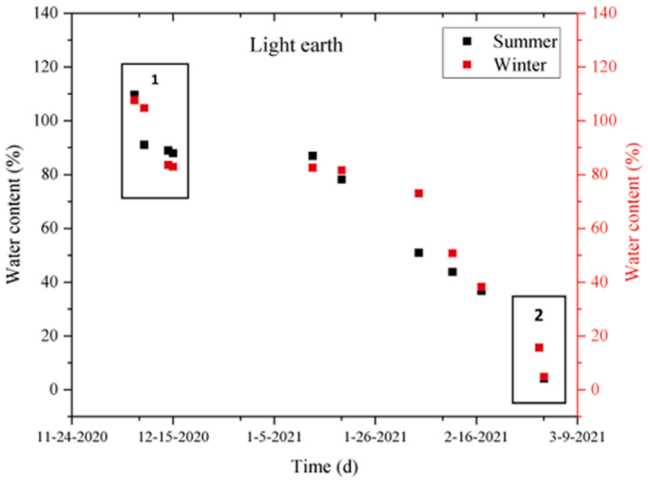

Fig. 15. Laboratory drying kinetics of light-earth material.

drying kinetics is observed. After three months, the samples became dry, with a stable water content of 4% (phase 2, Fig. 15).

3.3. Hygroscopic behavior

3.3.1. Sorption isotherm

The moisture sorption isotherms shown in Fig. 16 indicate the evolution of moisture content *versus* ambient air RH at a constant temperature of 23 °C for the cob and light-earth materials. According to Brunauer's proposal [59], the sorption curves correspond to type III and show hysteretic loops. This type of curve is typical among porous materials.

In the 10–30% RH range, the absorbed water vapor of cob and light-earth materials was observed to be between 0% and 2%. However, when the RH is 40–90%, the absorbed water vapor of the light-earth (2–9%) exceeds that of cob (0.5–2%), as shown in Fig. 16. To improve the analysis of this difference between the cob and light-earth materials, the raw materials (soils, reed fibers, and flax straw fibers) are characterized, as shown in Fig. 17. The results indicate that the sorption/desorption behavior of the cob is mainly regulated by soils 1 and 2 although it contains flax straw fibers with high water vapor absorption. However, because the flaw straw fiber content is only 2.5%, its impact is not apparent. The sorption/desorption behavior of light-earth materials is primarily governed by the presence of reed fibers.

According to the mixing law of components, Eqs. (8) and (9) are used to calculate the mass difference between cob and light-earth materials as a function of the percentage of components [28]. The two curves of cob and light-earth are plotted and compared, as shown in Fig. 18.

$$M_{Cob(Lawmix)} = 0.025M_{Flaxstrawfibre} + 0.325M_{soil1} + 0.65M_{Soil2} \tag{8}$$

$$M_{Lightearth(Lawmix)} = 0.35M_{reedfibre} + 0.65M_{Soil3} \tag{9}$$

The curves in Fig. 18 indicate that for light-earth, the mass difference between the sample and mixture is negligible. This occurs probably due to the moisture absorption provided by the reed fibers, which can influence the mixing law calculation. In contrast, the porosity (which is related to compaction) of the light-earth sample.

For the cob, a significant difference between the sample and mixture is observed because the porosity can impact the moisture absorption of the sample. In addition, the moisture absorption of the flax straw fibers exceeded that of the fibers covered by soil.

3.3.2. Open porosity

The values related to open porosity are listed in Table 6. These are correlated with the results of the sorption/desorption curves of the cob and light-earth materials. The low porosity of the cob reduces the area of hysteresis and therefore decreases its hygroscopic absorption of humidity. However, a more porous light-earth allows for better humidity absorption (Fig. 18).

The water absorption capacity of soil and fibers has an important effect on their adhesion to the matrix. Particle swelling, which is caused by water absorption during the first 24 h, pushes away soil. After drying, the volume of particles decreases, and voids form around them [60].

The sorption ability of the light-earth was observed to be better than that of the cob (Fig. 16). This means that light-earth can prevent moisture condensation pathology, and its surface is relevant for evaluating heat flux. The hygroscopic property of light-earth materials is well observed; however, that of cob materials is less well known.

This property is advantageous for the two mixes; however, it may increase the moisture content inside the material, influencing its durability, strength, and thermal insulation properties. In view of this, the investigation of the water vapor permeability of cob and light-earth materials is important.

3.3.3. Water vapor permeability

The measurement results of the cob and light-earth materials are listed in Table 7. The water vapor resistance factors are 12.9 and 8.2 for the cob and light-earth, respectively. The cob presents a 36% higher factor compared with the light-earth material. Consequently, the light-earth material remains more hygroscopic than the cob material. As for sorption/desorption, the lower water vapor permeability of the cob is due to the reduced open porosity. This low permeability is also due to the nature of the connection between the soils and flax straw that did not generate a sufficient quantity of voids for the storage of absorbed water vapor. In contrast, the water vapor permeability of light-earth exceeds that of cob due to the increase in porosity and nature of the reed. This renders the hygroscopic character of light-earth better than that of cob (Fig. 19).

3.4. Thermal conductivity

The results of the monitoring of cob and light-earth materials in climatic chambers under winter and summer conditions are analyzed. Using the foregoing, plots that define the relationship between thermal conductivity and density are produced (Fig. 20 and Fig. 21), and they are showed in the following paragraphs. These plots enable the estimation of the thermal conductivity of cob and light-earth depending on the water content and open porosity.

3.4.1. Cob measurement

As presented in Fig. 20, the drying kinetics of the cob under summer and winter conditions are similar, with a decrease in density from 2200 to 1600 kg/m^3; the final water content of the samples is 3%. Notably, the mass loss of the samples was not homogenous; it

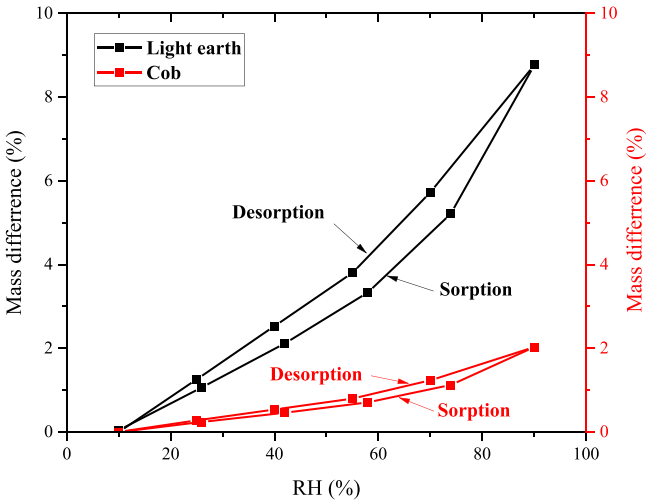

Fig. 16. Moisture sorption isotherm of cob and light-earth materials.

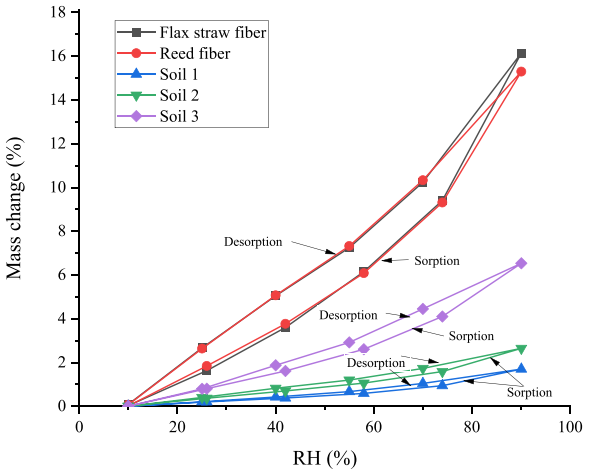

Fig. 17. Moisture sorption isotherm of soils and fibers.

decreased by 1% initially and by 17% overall.

The thermal conductivity decreased as the water contents decreased from 1.31 to 0.48 W•m^{-1}•K^{-1} in summer and from 1.27 to 0.58 W•m^{-1}•K^{-1} in winter (Fig. 21).

3.4.2. Light-earth measurement

As shown in Fig. 22, the drying kinetics of light-earth under summer and winter conditions are similar, decreasing in density from of 1000–600 kg/m^3; the final water content is 4%.

The thermal conductivity decreased as the water contents decreased from 0.50 to 0.13 W•m^{-1}•K^{-1} in summer and from 0.40 to 0.14 W•m^{-1}•K^{-1} in winter (Fig. 23).

4. Literature comparison

To be able to evaluate the performance of the cob and lightened earth, their hygrothermal behavior is compared to the literature. In Table 8, the hygrothermal properties of different earth-based materials are reported: light earth of different densities, cob, earth bricks, *etc.* It should be mentioned that the reported properties were obtained under experimental conditions (temperature and relative humidity) which are sometimes different. This fact has not been considered in the present comparisons.

From the light earth section in Table 8, it can be seen that mixtures investigated in present study are hygroscopically and thermally (thermal conductivity) less efficient than those reported in other works [5,28,32]. This may mainly be due to the differences in the used materials and preparation/conditioning methods. In addition, differences in density can be observed. In fact, materials in present study

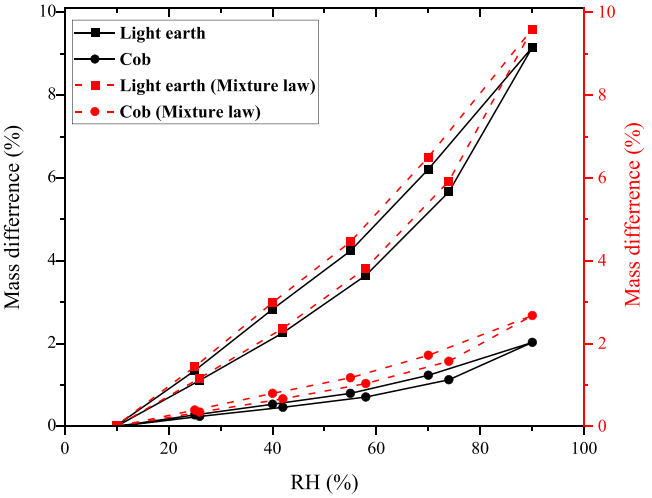

Fig. 18. Moisture sorption isotherm of cob and light-earth compared with mixture law.

Table 6
Open porosity measurement for cob and light-earth.

Materials	Cob			Light-earth		
Number of samples	1	2	3	1	2	3
Porosity "Φ" (%)	30	28	31	53	55	55
Mean porosity "Φ" (%)	30 ± 1			54 ± 1		

Table 7
Water vapor resistance factor (μ) of cob and light earth.

Materials	Cob			Light-earth		
Number of samples	1	2	3	1	2	3
δ: Water vapor permeability, $\times 10^{-12}$ (kg•m^{-1}•s^{-1}•Pa^{-1})	16.2	15.7	14.6	25.5	25.4	22.3
δ mean $\times 10^{-12}$ (kg•m^{-1}•s^{-1}•Pa^{-1})	15.5 ± 0.8			24.4 ± 1.9		
Water vapor resistance factor, μ (-)	12.35	12.72	13.75	7.8	7.9	9.0
μ mean (-)	12.9 ± 0.7			8.2 ± 0.7		

Fig. 19. Sample sections of cob (left) and light-earth (right).

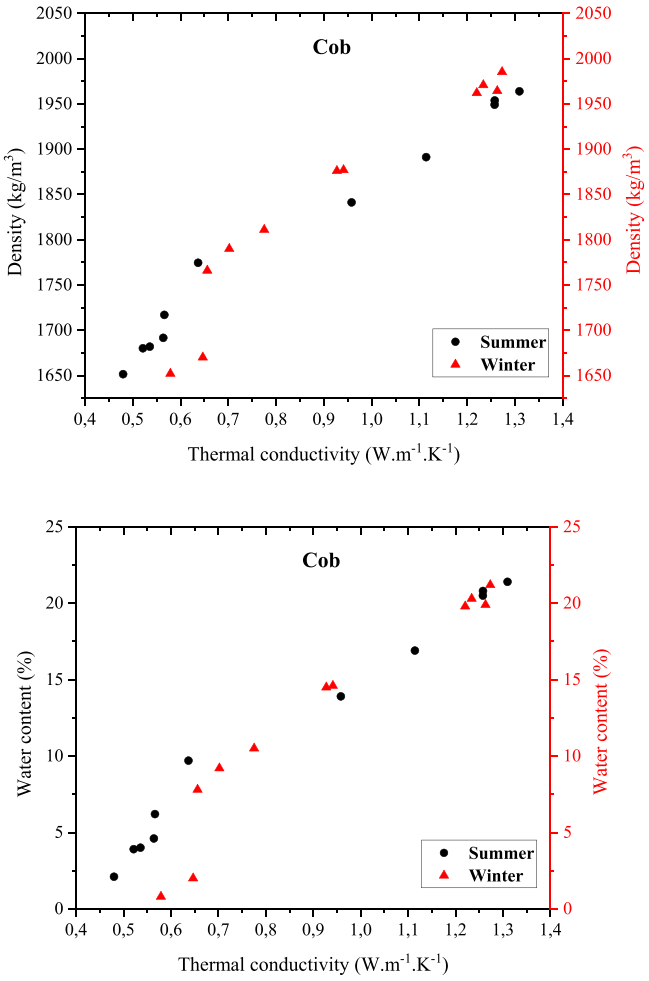

Fig. 20. Thermal conductivity of cob under winter and summer conditions (Laboratory).

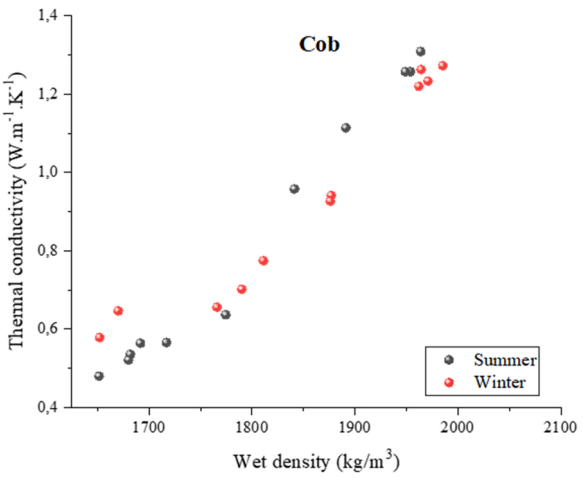

Fig. 21. Relationship between thermal conductivity and density of cob sample (laboratory).

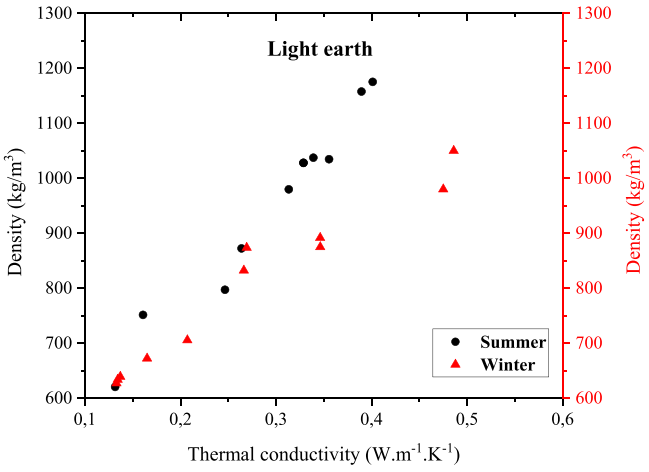

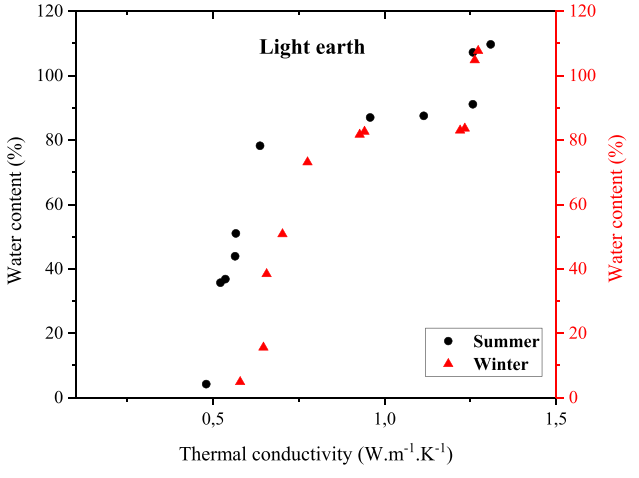

Fig. 22. Thermal conductivity of light-earth under winter and summer conditions (laboratory).

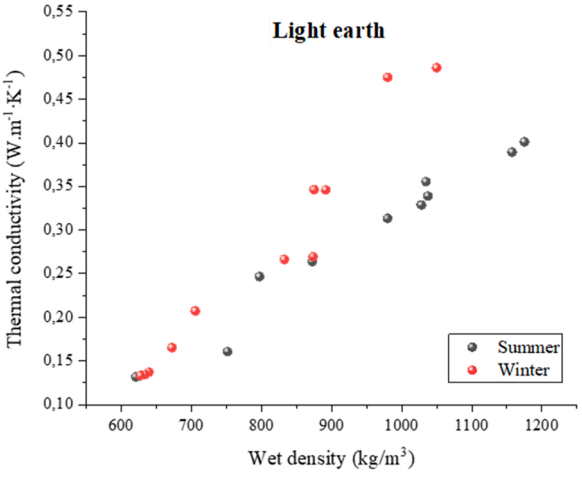

Fig. 23. Relationship between thermal conductivity and density of light-earth sample (laboratory).

Table 8
Hygrothermal properties for different earth-based materials.

Earth-based materials	References	Mix	Density [kg/m3]	Sorption max [%]	μ (Dry cup)	λ [W•m^{-1}•K^{-1}]
Light earth	Present study	Light earth (Earth + 35% Reed)	620	8.76 at RH = 90%	8.2	0.13–0.14 at 20 ∘C
	[5]	Earth + Straw	241–531	12 at RH = 93%	4.8	0.071–0.120 at 25 ∘C
	[33]	Earth + Typha Australis (20%, 33%)	323–586	12.9 at RH = 97%	3.75 – 7.06	0.06–0.11 at 23 ∘C
	[28]	Earth + hemp shiv 34–67%	200–350	5.3–7.5 at RH = 80%	2.24–4.14	0.06–0.12 at 23 ∘C
Cob	Present study	Cob (Earth + 2,5% flax staw)	1650	2 at RH = 90%	12.9	0.48–0.58 at 20 ∘C
	[48]	Cob	1462–2011	2.8–4.1 at RH = 90%	7–9.98	0.62–1.93
Other earth-based materials	[61]	Unfired earth bricks	1761–1797	5.3 at RH = 95%	–	0,77–0,95
	[24]	Extruded brick	1940–2070	4–6 At RH= 97%	7–9	0.47–0.59 at 25 °C

are denser when compared to those reported in Refs. [5,28,32]. This difference in density can explain, in part, the disparities between here-obtained results and those reported in literature. Indeed, this parameter is of a crucial importance. Niang et al. [33] reported that thermal conductivity increases from 0.06 to 0.11 W•m^{-1}•K^{-1} when light earth density increases from 323 to 586 kg/m^3. This increase in density also affects the light earth hygroscopic properties. In fact, maximum moisture sorption decreases, and water vapor resistance factor increases. Moreover, Colinart et al. [28] reported that thermal conductivity clearly increases with density. However, no effect of density on water vapor resistance factor was clearly observed.

Light earth hygroscopic proprieties are better than other earth-based materials considered as suitable to moderate buildings indoor humidity. In case of water vapor permeability, here investigated materials behave as Cob or earth bricks, see Table 8. Regarding maximum sorption value, light earth mixtures are more efficient when compared to these latter. Otherwise, due to their high fiber content, soil-fiber mixtures present a lower thermal conductivity than Cob or earth bricks.

From the cob section in Table 8, it can be seen that mixtures investigated in present study are hygroscopically less efficient than those reported in the work of Phung [48] but, thermally (thermal conductivity) is more efficient (0.48–0.58 W•m^{-1}•K^{-1}) than works of phung and [47,59].

5. Conclusion

This study focuses on understanding and quantifying the drying kinetics evolution and hygrothermal properties of cob and light-earth materials constituting a double-walling system of cob and light-earth. The experimental measurements were focused on moisture sorption isotherm, open porosity, and water vapor permeability.

The drying process in the cob and light-earth materials was found to follow an exponential decline function. An exception was observed in light-earth during the first week after construction. The VWC remained approximately constant probably due to the water absorbed by the reed fibers constituting the mix. In contrast, a variance in drying rate between the upper and lower parts of the same lift, especially in the cob, was observed. In addition, the initial *in situ* VWC was observed to be more homogeneous in cob than in light-earth. The initial drying kinetics *in situ* were similar to those in a climatic chamber simulation in the laboratory. It can be concluded that climatic chamber results exhibit good correlation with *in situ* studies.

The density and thermal conductivity of the cob and light-earth samples were measured under winter and summer conditions in climatic chambers simulation. The results revealed that the density of cob decreased from 2000 to 1600 kg/m^3; its thermal conductivity also decreased from 1.31 to 0.48 W•m^{-1}•K^{-1} in summer and from 1.27 to 0.58 W•m^{-1}•K^{-1} in winter. The density of light-earth decreased from 1000 kg to 600 kg/m^3; its thermal conductivity decreased from 0.50 to 0.13 W•m^{-1}•K^{-1} in summer and from 0.40 to 0.13 W•m^{-1}•K^{-1} in winter.

The hygrothermal results revealed a relationship between the thermal conductivity, density, and water content of cob and light-earth under summer and winter conditions. In addition, open porosity was found to affect water vapor permeability and sorption/desorption.

This study gives us perspectives to try to reproduce as well as possible the real conditions in laboratory. to continue the work in CobBauge project, other properties of these materials will be studied, in particular, the investigation of compaction and shrinkage of walls *in situ* which will be compared to laboratory results on small scale walls.

Declaration of Competing Interest

The authors declare that they have no known competing financial interests or personal relationships that could have appeared to influence the work reported in this paper.

Data Availability

Data will be made available on request.

Acknowledgements

This wo35rk was conducted under the CobBaugeproject selected by the European cross-border cooperation program INTERREG V France (Manche/Channel) England.

References

[1] G. Minke, Building with Earth: Design and Technology of a Sustainable Architecture, Birkhäuser, 2013. https://doi.org/10.1515/9783034612623.
[2] M. Barbuta, R.D. Bucur, S.M. Cimpeanu, G. Paraschiv, D. Bucur, Wastes in building materials industry, IntechOpen (2015), https://doi.org/10.5772/59933.
[3] E. Christoforou, A. Kylili, P.A. Fokaides, I. Ioannou, Cradle to site life cycle assessment (LCA) of adobe bricks, J. Clean. Prod. 112 (2016) 443–452, https://doi.org/10.1016/j.jclepro.2015.09.016.
[4] L. Ben-Alon, V. Loftness, K.A. Harries, G. DiPietro, E.C. Hameen, Cradle to site life cycle assessment (LCA) of natural vs conventional building materials: a case study on cob earthen material, Build. Environ. 160 (2019), 106150, https://doi.org/10.1016/j.buildenv.2019.05.028.
[5] M. Labat, C. Magniont, N. Oudhof, J.-E. Aubert, From the experimental characterization of the hygrothermal properties of straw-clay mixtures to the numerical assessment of their buffering potential, Build. Environ. 97 (2016) 69–81, https://doi.org/10.1016/j.buildenv.2015.12.004.
[6] M. Greer, D. Short, Aspect of composite behaviour of cob. A Seminar paper on out of Earth II. University of Plymouth., (1996).
[7] Medicine Institute of: Damp Indoor Spaces and Health, The National Academies Press, Washington, DC, 2004. https://doi.org/10.17226/11011.
[8] P.M. Bluyssen, towards an integrative approach of improving indoor air quality, Build. Environ. 44 (2009) 1980–1989, https://doi.org/10.1016/j.buildenv.2009.01.012.
[9] S. You, W. Li, T. Ye, F. Hu, W. Zheng, Study on moisture condensation on the interior surface of buildings in high humidity climate, Build. Environ. 125 (2017) 39–48, https://doi.org/10.1016/j.buildenv.2017.08.041.
[10] P.J. Annila, M. Hellemaa, T.A. Pakkala, J. Lahdensivu, J. Suonketo, M. Pentti, Extent of moisture and mould damage in structures of public buildings, Case Stud. Constr. Mater. 6 (2017) 103–108, https://doi.org/10.1016/j.cscm.2017.01.003.
[11] T. Pierre, T. Colinart, P. Glouannec, Measurement of thermal properties of biosourced building materials, Int. J. Thermophys. 35 (2014) 1832–1852, https://doi.org/10.1007/s10765-013-1477-0.
[12] L. Miccoli, U. Müller, P. Fontana, Mechanical behaviour of earthen materials: a comparison between earth block masonry, rammed earth and cob, Constr. Build. Mater. 61 (2014) 327–339, https://doi.org/10.1016/j.conbuildmat.2014.03.009.
[13] M. Moevus, Y. Jorand, C. Olagnon, S. Maximilien, R. Anger, L. Fontaine, L. Arnaud, Earthen construction: an increase of the mechanical strength by optimizing the dispersion of the binder phase, Mater. Struct. 49 (2016) 1555–1568, https://doi.org/10.1617/s11527-015-0595-5.
[14] D.D. Tripura, K.D. Singh, Mechanical behaviour of rammed earth column: a comparison between unreinforced, steel and bamboo reinforced columns, Mater. Construcc. 68 (2018), https://doi.org/10.3989/mc.2018.11517 e174–e174.
[15] L. Miccoli, R.A. Silva, D.V. Oliveira, U. Müller, Static behavior of cob: experimental testing and finite-element modeling, J. Mater. Civ. Eng. 31 (2019) 04019021, https://doi.org/10.1061/(ASCE)MT.1943-5533.0002638.
[16] H. Bui, N. Sebaibi, M. Boutouil, D. Levacher, Determination and review of physical and mechanical properties of raw and treated coconut fibers for their recycling in construction materials, Fibers 8 (2020) 37, https://doi.org/10.3390/fib8060037.
[17] A. Azil, M. Le Guern, K. Touati, N. Sebaibi, M. Boutouil, F. Streiff, S. Goodhew, M. Gomina, Earth construction: field variabilities and laboratory reproducibility, Constr. Build. Mater. 314 (2022), 125591, https://doi.org/10.1016/j.conbuildmat.2021.125591.
[18] Indian Standard.IS 13827, Indian Standard. IS 13827, 1993.
[19] Standards New Zealand:NZS 4298, Standards New Zealand, 1998. https://www.standards.govt.nz/shop/nzs-42981998.
[20] C.-S. Tang, B. Shi, C. Liu, W.-B. Suo, L. Gao, Experimental characterization of shrinkage and desiccation cracking in thin clay layer, Appl. Clay Sci. 52 (2011) 69–77, https://doi.org/10.1016/j.clay.2011.01.032.
[21] S. Sangma, D.D. Tripura, Experimental study on shrinkage behaviour of earth walling materials with fibers and stabilizer for cob building, Constr. Build. Mater. 256 (2020), 119449, https://doi.org/10.1016/j.conbuildmat.2020.119449.
[22] S. Sangma, D.D. Tripura, Characteristic properties of unstabilized, stabilized and fibre-reinforced cob blocks, Struct. Eng. Int. 31 (2021) 76–84, https://doi.org/10.1080/10168664.2019.1690957.
[23] S. Liuzzi, M.R. Hall, P. Stefanizzi, S.P. Casey, Hygrothermal behaviour and relative humidity buffering of unfired and hydrated lime-stabilised clay composites in a Mediterranean climate, Build. Environ. 61 (2013) 82–92, https://doi.org/10.1016/j.buildenv.2012.12.006.
[24] H. Cagnon, J.E. Aubert, M. Coutand, C. Magniont, Hygrothermal properties of earth bricks, Energy Build. 80 (2014) 208–217, https://doi.org/10.1016/j.enbuild.2014.05.024.
[25] L. Zhang, L. Yang, B.P. Jelle, Y. Wang, A. Gustavsen, Hygrothermal properties of compressed earthen bricks, Constr. Build. Mater. 162 (2018) 576–583, https://doi.org/10.1016/j.conbuildmat.2017.11.163.
[26] K.E. Azhary, S. Raefat, N. Laaroussi, M. Garoum, Energy performance and thermal proprieties of three types of unfired clay bricks, Energy Procedia 147 (2018) 495–502, https://doi.org/10.1016/j.egypro.2018.07.059.
[27] T. Vinceslas, T. Colinart, E. Hamard, A.H. de Ménibus, T. Lecompte, H. Lenormand, Light Earth erformances for thermal insulation: Application to Earth–Hemp, in: B.V.V. Reddy, M. Mani, P. Walker (Eds.), Earthen Dwellings and Structures: Current Status in Their Adoption, Springer, Singapore, 2019: pp. 357–367. https://doi.org/10.1007/978–981-13–5883-8_31.
[28] T. Colinart, T. Vinceslas, H. Lenormand, A.H.D. Menibus, E. Hamard, T. Lecompte, Hygrothermal properties of light-earth building materials, J. Build. Eng. 29 (2020), 101134, https://doi.org/10.1016/j.jobe.2019.101134.
[29] M. Posani, R. Veiga, V. Peixoto de Freitas, Thermal Renders for Traditional and Historic Masonry Walls: comparative study and recommendations for hygric compatibility, (n.d.).
[30] D. Allinson, M. Hall, Hygrothermal analysis of a stabilised rammed earth test building in the UK, Energy Build. 42 (2010) 845–852, https://doi.org/10.1016/j.enbuild.2009.12.005.
[31] T. Ashour, A. Korjenic, S. Korjenic, W. Wu, Thermal conductivity of unfired earth bricks reinforced by agricultural wastes with cement and gypsum, Energy Build. 104 (2015) 139–146, https://doi.org/10.1016/j.enbuild.2015.07.016.
[32] F. Volhard, Light Earth Building, A Handbook for Building with Wood and Earth; Birkhauser: Basel, Switzerland, 2016.
[33] I. Niang, C. Maalouf, T. Moussa, C. Bliard, E. Samin, C. Thomachot-Schneider, M. Lachi, H. Pron, T.H. Mai, S. Gaye, Hygrothermal performance of various Typha–clay composite, J. Build. Phys. 42 (2018) 316–335, https://doi.org/10.1177/1744259118759677.
[34] M. Le Guern, N. Sebaibi, M. Boutouil, Technical report Cobbauge project., ESITC Caen, 2018.
[35] T. Vinceslas, E. Hamard, A. Razakamanantsoa, F. Bendahmane, Further development of a laboratory procedure to assess the mechanical performance of cob, Environ. Geotech. 7 (2018) 200–207, https://doi.org/10.1680/jenge.17.00056.
[36] F.P. Incropera, D.P. DeWitt, Fundamentals of Heat and Mass Transfer, Wiley, New York, 2002.

[37] A. Fabbri, N. Al Haffar, F. McGregor, Measurement of the relative air permeability of compacted earth in the hygroscopic regime of saturation, Comptes Rendus Mécanique 347 (2019) 912–919, https://doi.org/10.1016/j.crme.2019.11.017.
[38] T. Zakri, J.-P. Laurent, M. Vauclin, Theoretical evidence for `Lichtenecker's mixture formulae' based on the effective medium theory, J. Phys. D: Appl. Phys. 31 (1998) 1589–1594, https://doi.org/10.1088/0022-3727/31/13/013.
[39] A. Azil, M.L. Guern, R. Rattier, K. Touati, N. Sebaibi, Y.E. Mendili, M. Boutouil, F. Streiff, S. Goodhew, H. Louahlia, Réalisation d'un bâtiment pilote en terre-fibres, Acad. J. Civ. Eng. 38 (2020) 165–168, https://doi.org/10.26168/ajce.38.1.40.
[40] A. Azil, M. Le Guern, K. Touati, M. Gomina, N. Sebaibi, M. Boutouil, F. Streiff, S. Goodhew, H. Louahlia, Construction filed monitoring of a cob prototype building, Constr. Technol. Archit. Vol. 1 (2022) 458–465.
[41] NF P94–06: soils investigation and testing. Measuring of the methylene blue adsorption capacity of à rocky soil. Determination of the methylene blue of à soil by means of the stain test., NF P94–068, 1998. https://sagaweb.afnor.org/fr-FR/sw/Consultation/Notice/1261353?directFromSearch=true.
[42] NF EN ISO 17892–12: Geotechnical investigation and testing - Laboratory testing of soil - Part 12: determination of liquid and plastic limits, NF EN ISO 17892–12, 2018. https://sagaweb.afnor.org/fr-FR/sw/Consultation/Notice/1446382?directFromSearch=true.
[43] NF P11–300: Earthworks. Classification of materials for use in the construction of embankments and capping layers of road infrastructures., n.d.
[44] ISO 17892–3: Geotechnical investigation and testing - Laboratory testing of soil - Part 3: determination of particle density, ISO 17892–3, 2015. https://viewerbdc.afnor.org/pdf/viewer/bc1WvkF_3UA1.
[45] XP P94–041: soil investigation and testing. Granulometric description. Wet sieving method., 1995. https://sagaweb.afnor.org/fr-FR/sw/Consultation/Notice/1260077?directFromSearch=true.
[46] ISO 13320: Particle size analysis - Laser diffraction methods, ISO 13320, 2020.
[47] NF P94–093: soils investigation and testing - Determination of the compaction reference values of a soil type - Standard proctor test - Modified proctor test, NF P94–093, 2014. https://sagaweb.afnor.org/fr-FR/sw/Consultation/Notice/1415768?directFromSearch=true.
[48] T.A. Phung, Formulation et caractérisation d'un composite terre-fibres végétales: la bauge, 2018.
[49] S. Amziane, F. Collet, M. Lawrence, C. Magniont, V. Picandet, M. Sonebi, Recommendation of the RILEM TC 236-BBM: characterisation testing of hemp shiv to determine the initial water content, water absorption, dry density, particle size distribution and thermal conductivity, Mater. Struct. 50 (2017), https://doi.org/10.1617/s11527-017-1029-3.
[50] ISO 11464: Soil quality - Pretreatment of samples for physico-chemical analysis, n.d. https://cobaz.afnor.org/notice/norme/iso-114642006/XS115126?rechercheID=2888172&searchIndex=1&activeTab=all#id_lang_2_Titles.
[51] NF X31–501: soil quality. Physical methods. Measuring of the bulk density of a undisturbed soil sample. Cylinder method, NF X31–501, 1992. https://sagaweb.afnor.org/fr-FR/sw/consultation/notice/1244134?recordfromsearch=True.
[52] P.-A. Chabriac, A. Fabbri, J.-C. Morel, J.-P. Laurent, J. Blanc-Gonnet, A procedure to measure the in-situ hygrothermal behavior of earth walls, Mater. (Basel) 7 (2014) 3002–3020, https://doi.org/10.3390/ma7043002.
[53] T.G. Caldwell, T. Bongiovanni, M.H. Cosh, C. Halley, M.H. Young, Field and laboratory evaluation of the CS655 soil water content sensor, Vadose Zone J. 17 (2018), 170214, https://doi.org/10.2136/vzj2017.12.0214.
[54] ISO 12571: Hygrothermal performance of building materials and products - Determination of hygroscopic sorption properties, 2013. https://cobaz.afnor.org/notice/norme/iso-125712013/XS124286?rechercheID=2890777&searchIndex=2&activeTab=all#id_lang_2_Titles.
[55] NF EN ISO 12572: Hygrothermal performance of building materials and products - Determination of water vapour transmission properties - Cup method, NF EN ISO 12572, 2016. https://cobaz.afnor.org/notice/norme/nf-en-iso-12572/FA184538?rechercheID=2708475&searchIndex=1&activeTab=all#id_lang_1_descripteur.
[56] NF ISO 11464: Soil quality - Pretreatment of samples for physico-chemical analysis, n.d. https://cobaz.afnor.org/notice/norme/nf-iso-11464/FA134263?rechercheID=3517308&searchIndex=1&activeTab=all#id_lang_2_Titles.
[57] NF ISO 5017: Dense shaped refractory products - Determination of bulk density, apparent porosity and true porosity, NF ISO 5017, 2013. https://sagaweb.afnor.org/fr-FR/sw/Consultation/Notice/1400375?directFromSearch=true.
[58] G. Scheffler, R. Plagge, Introduction of a Drying Coefficient for Building Materials, (2010).
[59] R.D. Andrade, M.R. Lemus, C. Perez, Models of sorption isotherms for food: uses and limitations, Vitae 18 (2011) 325–334.
[60] M. Segetin, K. Jayaraman, X. Xu, Harakeke reinforcement of soil–cement building materials: manufacturability and properties, Build. Environ. 42 (2007) 3066–3079, https://doi.org/10.1016/j.buildenv.2006.07.033.
[61] D. Medjelekh, L. Ulmet, F. Dubois, Characterization of hygrothermal transfers in the unfired earth, Energy Procedia 139 (2017) 487–492, https://doi.org/10.1016/j.egypro.2017.11.242.